References

Ahmad, N., Rappaz, J., Desbiolles, J.-L., Jalanti, T., Rappaz, M., Combeau, H., Lesoult, G., and Stomp, C. (1998). Numerical simulation of macrosegregation: a comparison between finite volume method and finite element method predictions and a confrontation with experiments. *Metallurgical and Materials Transactions A*, 29(2):617–630.

Ahmadein, M., Wu, M., and Ludwig, A. (2015). Analysis of macrosegregation formation and columnar-to-equiaxed transition during solidification of al-4 wt.% cu ingot using a 5-phase model. *Journal of crystal growth*, 417:65–74.

Alkemper, J., Sous, S., Stöcker, C., and Ratke, L. (1998). Directional solidification in an aerogel furnace with high resolution optical temperature measurements. *Journal of crystal growth*, 191(1-2):252–260.

Anderson, D. and Worster, M. G. (1996). A new oscillatory instability in a mushy layer during the solidification of binary alloys. *Journal of Fluid Mechanics*, 307:245–267.

ANSYS, F. (2017). 18.1, user guide, ansys.

Assael, M. J., Kalyva, A. E., Antoniadis, K. D., Michael Banish, R., Egry, I., Wu, J., Kaschnitz, E., and Wakeham, W. A. (2010). Reference data for the density and viscosity of liquid copper and liquid tin. *Journal of Physical and Chemical Reference Data*, 39(3):033105.

Bennon, W. and Incropera, F. (1987a). A continuum model for momentum, heat and species transport in binary solid-liquid phase change systems—i. model formulation. *International Journal of Heat and Mass Transfer*, 30(10):2161–2170.

Bennon, W. and Incropera, F. (1987b). A continuum model for momentum, heat and species transport in binary solid-liquid phase change systems—ii. application to solidification in a rectangular cavity. *International Journal of Heat and Mass Transfer*, 30(10):2171–2187.

Bergman, M. I., Fearn, D. R., Bloxham, J., and Shannon, M. C. (1997). Convection and channel formation in solidifying pb- sn alloys. *Metallurgical and Materials Transactions A*, 28(13):859–866.

Bhattacharya, A. (2014). *Effect of Convection and Shrinkage on Solidification and Microstructure Formation*. PhD thesis, Department of Mechanical Engineering, Indian Institute of Science, Bangalore – 560012, India.

Bhattacharya, A. (2019). Binary alloy dendrite growth in presence of shrinkage induced convection. *Materials Research Express*, 6(12):126544.

Bhattacharya, A. and Dutta, P. (2014). Effect of shrinkage induced flow on binary alloy dendrite growth: An equivalent undercooling model. *International Communications in Heat and Mass Transfer*, 57:216–220.

Boettinger, W., Shechtman, D., Schaefer, R., and Biancaniello, F. (1984). The effect of rapid solidification velocity on the microstructure of ag-cu alloys. *Metallurgical transactions A*, 15(1):55–66.

Bounds, S., Moran, G., Pericleous, K., Cross, M., and Croft, T. (2000). A computational model for defect prediction in shape castings based on the interaction of free surface flow, heat transfer, and solidification phenomena. *Metallurgical and Materials Transactions B*, 31(3):515–527.

Brent, A., Voller, V. R., and Reid, K. (1988). Enthalpy-porosity technique for modeling convection-diffusion phase change: application to the melting of a pure metal. *Numerical Heat Transfer, Part A Applications*, 13(3):297–318.

Bridgman, P. W. (1931). Crystals and their manufacture. US Patent 1,793,672.

Cahill, J. and Kirshenbaum, A. (1962). The density of liquid copper from its melting point (1356° k.) to 2500° k. and an estimate of its critical constants1, 2. *The Journal of Physical Chemistry*,

66(6):1080–1082.
Chakraborty, P. R. (2017). Enthalpy porosity model for melting and solidification of pure-substances with large difference in phase specific heats. *International Communications in Heat and Mass Transfer*, 81:183–189.
Chakraborty, P. R. and Dutta, P. (2013). Study of freckles formation during directional solidification under the influence of single-phase and multiphase convection. *Journal of Thermal Science and Engineering Applications*, 5(2).
Chakraborty, P. R., Hiremath, K. R., and Sharma, M. (2017). Evaluation of evaporation coefficient for micro-droplets exposed to low pressure: A semi-analytical approach. *Physics Letters A*, 381(5):413–416.
Chakraborty, S. and Dutta, P. (2003). Analytical solutions for heat transfer during cyclic melting and freezing of a phase change material used in electronic or electrical packaging. *J. Electron. Packag.*, 125(1):126–133.
Chen, C. (1995). Experimental study of convection in a mushy layer during directional solidification. *Journal of Fluid Mechanics*, 293:81–98.
Chen, C. and Chen, F. (1991). Experimental study of directional solidification of aqueous ammonium chloride solution. *Journal of Fluid Mechanics*, 227:567–586.
Chen, F., Lu, J. W., and Yang, T. L. (1994). Convective instability in ammonium chloride solution directionally solidified from below. *Journal of Fluid Mechanics*, 276:163–187.
Chen, J. and Tsai, H.-L. (1993). Inverse segregation for a unidirectional solidification of aluminum-copper alloys. *International journal of heat and mass transfer*, 36(12):3069–3075.
Chen, K.-X. and Shen, H.-F. (2019). Numerical simulation of macrosegregation caused by thermal–solutal convection and solidification shrinkage using ale model. *Acta Metallurgica Sinica (English Letters)*, 32(11):1396–1406.
Chen, T. and Zhang, Y. (2006). Three-dimensional modeling of selective laser sintering of two-component metal powder layers.
Chiang, K. and Tsai, H. (1992a). Interaction between shrinkage-induced fluid flow and natural convection during alloy solidification. *International journal of heat and mass transfer*, 35(7):1771–1778.
Chiang, K. and Tsai, H.-L. (1992b). Shrinkage-induced fluid flow and domain change in two-dimensional alloy solidification. *International journal of heat and mass transfer*, 35(7):1763–1770.
Chiareli, A., Huppert, H. E., and Worster, M. G. (1994). Segregation and flow during the solidification of alloys. *Journal of crystal growth*, 139(1-2):134–146.
Chiareli, A. and Worster, M. G. (1995). Flow focusing instability in a solidifying mushy layer. *Journal of Fluid Mechanics*, 297:293–305.
Chung, C. and Worster, M. G. (2002). Steady-state chimneys in a mushy layer. *Journal of Fluid Mechanics*, 455:387.
Dagner, J., Friedrich, J., and Müller, G. (2008). Numerical study on the prediction of microstructure parameters by multi-scale modeling of directional solidification of binary aluminum–silicon alloys. *Computational materials science*, 43(4):872–885.
Dantzig, J. A. and Rappaz, M. (2016). *Solidification: -Revised & Expanded*. EPFL press.
Das, S., Krishna, R. M., Ma, S., and Mandal, K. C. (2013). Single phase polycrystalline cu2znsns4 grown by vertical gradient freeze technique. *Journal of crystal growth*, 381:148–152.
De Sousa, F., Mangiavacchi, N., Nonato, L., Castelo, A., Tomé, M. F., Ferreira, V., Cuminato, J., and McKee, S. (2004). A front-tracking/front-capturing method for the simulation of 3d multi-fluid flows with free surfaces. *Journal of Computational Physics*, 198(2):469–499.
Diao, Q. and Tsai, H.-L. (1993). Modeling of solute redistribution in the mushy zone during solidification of aluminum-copper alloys. *Metallurgical transactions A*, 24(4):963–973.
Dinsdale, A. and Quested, P. (2004). The viscosity of aluminium and its alloys–a review of data and models. *Journal of materials science*, 39(24):7221–7228.

Dorschu, K. (1968). Control of cooling rates in steel weld metal. *Welding Journal*, 47(2):S49.

Du, Q., Eskin, D., Jacot, A., and Katgerman, L. (2007). Two-dimensional modelling and experimental study on microsegregation during solidification of an al–cu binary alloy. *Acta materialia*, 55(5):1523–1532.

Du, Q. and Jacot, A. (2005). A two-dimensional microsegregation model for the description of microstructure formation during solidification in multicomponent alloys: Formulation and behaviour of the model. *Acta Materialia*, 53(12):3479–3493.

Dutta, P., Joshi, Y., and Janaswamy, R. (1995). Thermal modeling of gas tungsten arc welding process with nonaxisymmetric boundary conditions. *Numerical Heat Transfer, Part A: Applications*, 27(5):499–518.

Emms, P. and Fowler, A. (1994). Compositional convection in the solidification of binary alloys. *Journal of Fluid Mechanics*, 262:111–139.

Eskin, D., Du, Q., Ruvalcaba, D., and Katgerman, L. (2005). Experimental study of structure formation in binary al–cu alloys at different cooling rates. *Materials Science and Engineering: A*, 405(1-2):1–10.

Evans, J., Beech, J., and Kirkwood, D. (1992). The prediction of shrinkage cavities in cast-steel rolls. *Cast Metals*, 5(3):130–140.

Felicelli, S. D., Heinrich, J., and Poirier, D. R. (1991). Simulation of freckles during vertical solidification of binary alloys. *Metallurgical and Materials Transactions B*, 22(6):847–859.

Fernández, M. C., Založnik, M., Combeau, H., and Hecht, U. (2020). Thermosolutal convection and macrosegregation during directional solidification of tial alloys in centrifugal casting. *International Journal of Heat and Mass Transfer*, 154:119698.

Ferreira, I. L., Santos, C. A., Garcia, A., and Voller, V. R. (2004). Analytical, numerical, and experimental analysis of inverse macrosegregation during upward unidirectional solidification of al-cu alloys. *Metallurgical and Materials Transactions B*, 35(2):285–297.

Ferreira, I. L., Spinelli, J. E., and Garcia, A. (2009). Gravity-driven inverse segregation during transient upward directional solidification of sn–pb hypoeutectic alloys. *Journal of Alloys and compounds*, 475(1-2):396–400.

Fisher, K. (1981). The effects of fluid flow on the solidification of industrial castings and ingots. *PhysicoChemical Hydrodynamics*, 2(4):311–326.

Flemings, M. C. (1974). Solidification processing. *Metallurgical transactions*, 5(10):2121–2134.

Fluent, A. (2017). 18.1, theory guide, ansys.

Gandin, C.-A. (2000a). Experimental study of the transition from constrained to unconstrained growth during directional solidification. *ISIJ international*, 40(10):971–979.

Gandin, C.-A. (2000b). From constrained to unconstrained growth during directional solidification. *Acta Materialia*, 48(10):2483–2501.

Gao, Z., Jie, W., Liu, Y., and Luo, H. (2017). Solidification modelling for coupling prediction of porosity and segregation. *Acta Materialia*, 127:277–286.

Gao, Z., Jie, W., Liu, Y., Zheng, Y., and Luo, H. (2019). A model for coupling prediction of inverse segregation and porosity for up-vertical unidirectional solidification of al–cu alloys. *Journal of Alloys and Compounds*, 797:514–522.

Ge, H., Ren, F., Li, J., Han, X., Xia, M., and Li, J. (2017). Four-phase dendritic model for the prediction of macrosegregation, shrinkage cavity, and porosity in a 55-ton ingot. *Metallurgical and Materials Transactions A*, 48(3):1139–1150.

Geng, S., Jiang, P., Shao, X., Mi, G., Wu, H., Ai, Y., Wang, C., Han, C., Chen, R., Liu, W., et al. (2018). Effects of back-diffusion on solidification cracking susceptibility of al-mg alloys during welding: A phase-field study. *Acta Materialia*, 160:85–96.

Gerlach, D., Tomar, G., Biswas, G., and Durst, F. (2006). Comparison of volume-of-fluid methods for surface tension-dominant two-phase flows. *International Journal of Heat and Mass Transfer*, 49(3-4):740–754.

Giamei, A. and Tschinkel, J. (1976). Liquid metal cooling: a new solidification technique.

Metallurgical transactions A, 7(9):1427–1434.
Gokhale, A. and Patel, G. (2005). Analysis of variability in tensile ductility of a semi-solid metal cast a356 al-alloy. *Materials Science and Engineering: A*, 392(1-2):184–190.
Guba, P. and Anderson, D. M. (2014). Diffusive and phase change instabilities in a ternary mushy layer. *Journal of fluid mechanics*, 760:634–669.
Guba, P. and Worster, M. G. (2010). Interactions between steady and oscillatory convection in mushy layers. *Journal of fluid mechanics*, 645:411.
Gudibande, N. and Iyer, K. (2016). Thermal shrinkage–based model for predicting the voids during solidification of lead. *Nuclear Technology*, 196(3):674–683.
Guo, J. and Beckermann, C. (2003). Three-dimensional simulation of freckle formation during binary alloy solidification: effect of mesh spacing. *Numerical Heat Transfer: Part A: Applications*, 44(6):559–576.
Harlow, F. H. and Welch, J. E. (1965). Numerical calculation of time-dependent viscous incompressible flow of fluid with free surface. *The physics of fluids*, 8(12):2182–2189.
Hattori, T., Bartos, N., Norris, S., Kirkpatrick, M., and Armfield, S. (2013). Experimental and numerical investigation of unsteady behaviour in the near-field of pure thermal planar plumes. *Experimental thermal and fluid science*, 46:139–150.
Hebditch, D. and Hunt, J. (1974). Observations of ingot macrosegregation on model systems. *Metallurgical transactions*, 5(7):1557–1564.
Heinrich, J., Sajja, U., Felicelli, S., and Westra, D. (2008). Projection method for flows with large local density gradients: application to dendritic solidification. *International journal for numerical methods in fluids*, 57(9):1211–1226.
Hemanth, J. (1999). Effect of cooling rate on dendrite arm spacing (das), eutectic cell count (ecc) and ultimate tensile strength (uts) of austempered chilled ductile iron. *Materials & Design*, 21(1):1–8.
Hirt, C. W. and Nichols, B. D. (1981). Volume of fluid (vof) method for the dynamics of free boundaries. *Journal of computational physics*, 39(1):201–225.
Hosseini, V., Shabestari, S., and Gholizadeh, R. (2013). Study on the effect of cooling rate on the solidification parameters, microstructure, and mechanical properties of lm13 alloy using cooling curve thermal analysis technique. *Materials & Design*, 50:7–14.
Jain, J., Kumar, A., and Dutta, P. (2007). Numerical studies on channel formation and growth during solidification: effect of process parameters.
Jamgotchian, H., Thi, H. N., Bergeon, N., and Billia, B. (2004). Double-diffusive convective modes and induced microstructure localisation during solidification of binary alloys. *International journal of thermal sciences*, 43(8):769–777.
Kashchiev, D. (2003). Determining the curvature dependence of surface tension. *The Journal of chemical physics*, 118(20):9081–9083.
Kasperovich, G., Volkmann, T., Ratke, L., and Herlach, D. (2008). Microsegregation during solidification of an al-cu binary alloy at largely different cooling rates (0.01 to 20,000 k/s): modeling and experimental study. *Metallurgical and Materials Transactions A*, 39(5):1183–1191.
Kato, H. and Cahoon, J. (1985). Inverse segregation in directionally solidified al-cu-ti alloys with equiaxed grains. *Metallurgical transactions A*, 16(4):579–587.
Katz, R. F. and Worster, M. G. (2008). Simulation of directional solidification, thermochemical convection, and chimney formation in a hele-shaw cell. *Journal of Computational Physics*, 227(23):9823–9840.
Kefayati, G. (2019). Lattice boltzmann simulation of double-diffusive natural convection of viscoplastic fluids in a porous cavity. *Physics of Fluids*, 31(1):013105.
Kim, C.-J. and Ro, S. (1993). Shrinkage formation during the solidification process in an open rectangular cavity. *Journal of heat transfer*, 115(4):1078–1081.
Kothe, D., Mjolsness, R., and Torrey, M. (1991). A computer program for incompressible flows with free surface. *Los Alamos National Lab. Los Alamos*.
Krane, M. J. M. and Incropera, F. P. (1995). Analysis of the effect of shrinkage on macrosegregation

in alloy solidification. *Metallurgical and Materials Transactions A*, 26(9):2329–2339.

Kumar, V., Abhishek, G. S., Srivastava, A., and Karagadde, S. (2020). On the mechanism responsible for unconventional thermal behaviour during freezing. *Journal of Fluid Mechanics*, 903:A32.

Kumar, V., Kumawat, M., Srivastava, A., and Karagadde, S. (2017). Mechanism of flow reversal during solidification of an anomalous liquid. *Physics of Fluids*, 29(12):123603.

Kumar, V., Srivastava, A., and Karagadde, S. (2018a). Compositional dependency of double-diffusive layers during binary alloy solidification: Full-field measurements and quantification. *Physics of Fluids*, 30(11):113603.

Kumar, V., Srivastava, A., and Karagadde, S. (2018b). Do the intrusive probes alter the characteristic length-scales of natural convection? *J. Flow Visualization Image Process*, 25:207.

Kumar, V., Srivastava, A., and Karagadde, S. (2018c). Real-time observations of density anomaly driven convection and front instability during solidification of water. *Journal of Heat Transfer*, 140(4).

Kumar, V., Srivastava, A., and Karagadde, S. (2019). Generalized regimes for the formation of stratified regions during freezing of multi-component mixtures. *Physics of Fluids*, 31(12):123602.

Lee, Z.-H., Lee, B., Kang, M., Chung, S., and Coriell, S. (1994). Experimental investigation of convection during vertical bridgman growth of dilute al-mg alloys. *Journal of crystal growth*, 141(1-2):209–218.

Li, X., Gagnoud, A., Ren, Z., Fautrelle, Y., and Moreau, R. (2009). Investigation of thermoelectric magnetic convection and its effect on solidification structure during directional solidification under a low axial magnetic field. *Acta materialia*, 57(7):2180–2197.

Liao, H., Sun, Y., and Sun, G. (2002). Correlation between mechanical properties and amount of dendritic α-al phase in as-cast near-eutectic al–11.6% si alloys modified with strontium. *Materials Science and Engineering: A*, 335(1):62–66.

Liu, J., Duarte, H. P., and Kou, S. (2017). Evidence of back diffusion reducing cracking during solidification. *Acta Materialia*, 122:47–59.

Lopez, J. M. and Marques, F. (2013). Instability of plumes driven by localized heating. *Journal of fluid mechanics*, 736:616–640.

Lopez, V., Scoles, A., and Kennedy, A. (2003). The thermal stability of tic particles in an al7wt.% si alloy. *Materials Science and Engineering: A*, 356(1-2):316–325.

Lukens, W., Morris, R., and Dunn, E. (1981). Infrared temperature sensing of cooling rates for arc welding control. Technical report, David W Taylor Naval Ship Research and Development Center Annapolis MD Ship Materials Engineering Dept.

Magnusson, T. and Arnberg, L. (2001). Density and solidification shrinkage of hypoeutectic aluminum-silicon alloys. *Metallurgical and Materials Transactions A*, 32(10):2605–2613.

Mo, A. and Thevik, H. J. (1998). Simplified computation of macrosegregation in multicomponent aluminum alloys. *Metallurgical and Materials Transactions A*, 29(8):2189–2194.

Monde, A. D., Chawla, O., Kumar, V., Karagadde, S., and Chakraborty, P. R. (2020). Shrinkage induced flow during directional solidification of pure substance in a bottom cooled cavity: A study on flow reversal phenomena. *Physics of Fluids*, 32(4):047104.

Motakef, S. (1990). Magnetic field elimination of convective interference with segregation during vertical-bridgman growth of doped semiconductors. *Journal of crystal growth*, 104(4):833–850.

Mullin, J. and Nỳvlt, J. (1971). Programmed cooling of batch crystallizers. *Chemical Engineering Science*, 26(3):369–377.

Narski, J. and Picasso, M. (2007). Adaptive finite elements with high aspect ratio for dendritic growth of a binary alloy including fluid flow induced by shrinkage. *Computer methods in applied mechanics and engineering*, 196(37-40):3562–3576.

Natale, M. F., Marcus, E. A. S., and Tarzia, D. A. (2010). Explicit solutions for one-dimensional two-phase free boundary problems with either shrinkage or expansion. *Nonlinear Analysis: Real World Applications*, 11(3):1946–1952.

Ni, J. and Beckermann, C. (1991). A volume-averaged two-phase model for transport phenomena during solidification. *Metallurgical Transactions B*, 22(3):349.

Nichols, B., Hirt, W., Hotchkiss, R., et al. (1980). A solution algorithm for transient fluid flow with multiple free boundaries. *Los Alamos National Laboratory, Technical Report, La-8355*.

Niu, X., Zhao, J., and Wang, B. (2019). Application of smooth particle hydrodynamics (sph) method in gravity casting shrinkage cavity prediction. *Computational Particle Mechanics*, 6(4):803–810.

Ozisik, M. N. (2002). *Boundary value problems of heat conduction*. Courier Corporation.

Patankar, S. (2018). *Numerical heat transfer and fluid flow*. Taylor & Francis.

Peppin, S., Huppert, H. E., and Worster, M. G. (2008). Steady-state solidification of aqueous ammonium chloride. *Journal of Fluid Mechanics*, 599:465.

Pequet, C., Rappaz, M., and Gremaud, M. (2002). Modeling of microporosity, macroporosity, and pipe-shrinkage formation during the solidification of alloys using a mushy-zone refinement method: applications to aluminum alloys. *Metallurgical and Materials Transactions A*, 33(7):2095–2106.

Prescott, P. and Incropera, F. (1993). Magnetically damped convection during solidification of a binary metal alloy.

Puckett, E. G., Almgren, A. S., Bell, J. B., Marcus, D. L., and Rider, W. J. (1997). A high-order projection method for tracking fluid interfaces in variable density incompressible flows. *Journal of computational physics*, 130(2):269–282.

Raabe, D. (1998). Computational materials science-the simulation of materials microstructures and properties.

Raessi, M. and Mostaghimi, J. (2005). Three-dimensional modelling of density variation due to phase change in complex free surface flows. *Numerical Heat Transfer, Part B: Fundamentals*, 47(6):507–531.

Raj, P. M., Sarkar, S., Chakraborty, S., Phanikumar, G., Dutta, P., and Chattopadhyay, K. (2002). Modelling of transport phenomena in laser surface alloying with distributed species mass source. *International journal of heat and fluid flow*, 23(3):298–307.

Rappaz, M. and Dantzig, J. A. (2009). *Solidification*. EPFL Press.

Reis, A., Xu, Z., Tol, R., and Neto, R. (2012). Modelling feeding flow related shrinkage defects in aluminum castings. *Journal of manufacturing processes*, 14(1):1–7.

Rerko, R. S., Beckermann, C., et al. (2003). Effect of melt convection and solid transport on macrosegregation and grain structure in equiaxed al–cu alloys. *Materials Science and Engineering: A*, 347(1-2):186–197.

Riahi, D. N. (1997). Effects of centrifugal and coriolis forces on chimney convection during alloy solidification. *Journal of crystal growth*, 179(1-2):287–296.

Roy, K., Ponalagusamy, R., and Murthy, P. (2020). The effects of double-diffusion and viscous dissipation on the oscillatory convection in a viscoelastic fluid saturated porous layer. *Physics of Fluids*, 32(9):094108.

Sajja, U. K. and Felicelli, S. D. (2011). Modeling freckle segregation with mesh adaptation. *Metallurgical and Materials Transactions B*, 42(6):1118–1129.

Sarazin, J. and Hellawell, A. (1988). Channel formation in Pb-Sn, Pb-Sb, and Pb-Sn-Sb alloy ingots and comparison with the system NH_4 Cl-H_2O. *Metallurgical Transactions A*, 19(7):1861–1871.

Sarkar, S., Raj, P. M., Chakraborty, S., and Dutta, P. (2002). Three-dimensional computational modeling of momentum, heat, and mass transfer in a laser surface alloying process. *Numerical Heat Transfer: Part A: Applications*, 42(3):307–326.

Sarreal, J. and Abbaschian, G. (1986). The effect of solidification rate on microsegregation. *Metallurgical Transactions A*, 17(11):2063–2073.

Satbhai, O., Roy, S., Ghosh, S., Chakraborty, S., and Lakkaraju, R. (2019). Comparison of the quasi-steady-state heat transport in phase-change and classical rayleigh-bénard convection for a wide range of stefan number and rayleigh number. *Physics of Fluids*, 31(9):096605.

Schulze, T. and Worster, M. G. (1998). A numerical investigation of steady convection in mushy layers during the directional solidification of binary alloys. *Journal of Fluid Mechanics*, 356:199–220.

Stansby, P. K. (2003). Solitary wave run up and overtopping by a semi-implicit finite-volume shallow-water boussinesq model. *Journal of Hydraulic Research*, 41(6):639–647.

Stefanescu, D. M. (2015). *Science and engineering of casting solidification*. Springer.

Sun, D. and Garimella, S. V. (2007). Numerical and experimental investigation of solidification shrinkage. *Numerical Heat Transfer, Part A: Applications*, 52(2):145–162.

Sung, P., Poirier, D. R., and Felicelli, S. (2001). Sensitivity of mesh spacing on simulating macrosegregation during directional solidification of a superalloy. *International journal for numerical methods in fluids*, 35(3):357–370.

Sussman, M., Fatemi, E., Smereka, P., and Osher, S. (1998). An improved level set method for incompressible two-phase flows. *Computers & Fluids*, 27(5-6):663–680.

Swaminathan, C. and Voller, V. (1992). A general enthalpy method for modeling solidification processes. *Metallurgical transactions B*, 23(5):651–664.

Swaminathan, C. and Voller, V. (1993). On the enthalpy method. *International Journal of Numerical Methods for Heat & Fluid Flow*, 3(3):233–244.

Taha, M. A., El-Mahallawy, N. A., and Hamouda, R. M. (2002). Relationship between formability and cast structures in end-chill directionally solidified al–cu alloys. *Materials & design*, 23(2):195–200.

Timms, R. (1985). Physical properties of oils and mixtures of oils. *Journal of the American Oil Chemists' Society*, 62(2):241–249.

Tingquist, S. and Laux, E. (1974). Method and apparatus for melting and casing metal. US Patent 3,841,384.

Trivedi, R., Liu, S., Mazumder, P., and Simsek, E. (2001). Microstructure development in the directionally solidified al–4.0 wt% cu alloy system. *Science and technology of Advanced Materials*, 2(1):309–320.

Tryggvason, G., Bunner, B., Esmaeeli, A., Juric, D., Al-Rawahi, N., Tauber, W., Han, J., Nas, S., and Jan, Y.-J. (2001). A front-tracking method for the computations of multiphase flow. *Journal of Computational Physics*, 169(2):708–759.

Unverdi, S. O. and Tryggvason, G. (1992). A front-tracking method for viscous, incompressible, multi-fluid flows. *Journal of computational physics*, 100(1):25–37.

Versteeg, H. K. and Malalasekera, W. (2007). *An introduction to computational fluid dynamics: the finite volume method*. Pearson education.

Voller, V., Swaminathan, C., and Thomas, B. G. (1990). Fixed grid techniques for phase change problems: a review. *International Journal for Numerical Methods in Engineering*, 30(4):875–898.

Voller, V. R., Cross, M., and Markatos, N. (1987). An enthalpy method for convection/diffusion phase change. *International journal for numerical methods in engineering*, 24(1):271–284.

Voller, V. R. and Prakash, C. (1987). A fixed grid numerical modelling methodology for convection-diffusion mushy region phase-change problems. *International Journal of Heat and Mass Transfer*, 30(8):1709–1719.

Wang, T., Wu, M., Ludwig, A., Abondano, M., Pustal, B., and Bu «hrig-Polaczek, A. (2005). Modelling the thermosolutal convection, shrinkage flow and grain movement of globular equiaxed solidification using a three phase model. *International Journal of Cast metals research*, 18(4):221–228.

Willers, B., Eckert, S., Nikrityuk, P. A., Räbiger, D., Dong, J., Eckert, K., and Gerbeth, G. (2008). Efficient melt stirring using pulse sequences of a rotating magnetic field: Part ii. application to solidification of al-si alloys. *Metallurgical and Materials Transactions B*, 39(2):304–316.

Worster, M. G. (1986). Solidification of an alloy from a cooled boundary. *Journal of Fluid Mechanics*, 167:481–501.

Worster, M. G. (1991). Natural convection in a mushy layer. *Journal of fluid mechanics*, 224:335–359.

Worster, M. G. (1992). Instabilities of the liquid and mushy regions during solidification of alloys.

Journal of Fluid Mechanics, 237:649–669.
Worster, M. G. and Kerr, R. C. (1994). The transient behaviour of alloys solidified from below prior to the formation of chimneys. *Journal of Fluid Mechanics*, 269:23–44.
Xiao, B. and Zhang, Y. (2006). Partial melting and resolidification of metal powder in selective laser sintering. *Journal of thermophysics and heat transfer*, 20(3):439–448.
Xie, J.-H., Julien, K., and Knobloch, E. (2020). Fixed-flux salt-finger convection in the small diffusivity ratio limit. *Physics of Fluids*, 32(12):126601.
Xu, D. and Li, Q. (1991). Gravity-and solidification-shrinkage-induced liquid flow in a horizontally solidified alloy ingot. *Numerical Heat Transfer*, 20(2):203–221.
Yang, H. (1992). Buckling of a thermal plume. *International journal of heat and mass transfer*, 35(6):1527–1532.
Zhang, B., Chen, W., and Poirier, D. (2000). Effect of solidification cooling rate on the fatigue life of a356. 2-t6 cast aluminium alloy. *Fatigue and Fracture of Engineering Materials and Structures*, 23(5):417–423.
Zhang, L., Jiang, Y., Ma, Z., Shan, S., Jia, Y., Fan, C., and Wang, W. (2008). Effect of cooling rate on solidified microstructure and mechanical properties of aluminium-a356 alloy. *Journal of materials processing technology*, 207(1-3):107–111.
Zhang, X., Wang, L.-l., Zhu, H., and Zeng, C. (2020). Modeling of salt finger convection through a fluid-saturated porous interface: Representative elementary volume scale simulation and effect of initial buoyancy ratio. *Physics of Fluids*, 32(8):082109.
Zhang, Y. and Faghri, A. (1999). Melting of a subcooled mixed powder bed with constant heat flux heating. *International Journal of Heat and Mass Transfer*, 42(5):775–788.
Zhuang, L. and Langer, E. (1989). Effects of cooling rate control during the solidification process on the microstructure and mechanical properties of cast co-cr-mo alloy used for surgical implants. *Journal of materials science*, 24(2):381–388.
Ziv, I. and Weinberg, F. (1989). The columnar-to-equiaxed transition in al 3 pct cu. *Metallurgical Transactions B*, 20(5):731–734.

Appendix A: Derivation of energy conservation equation as scalar variable temperature

1 ENERGY EQUATION FOR PURE AND ALLOY SYSTEM WITHOUT INTEGRATING FREE SURFACE

The energy conservation equation is derived on the basis of volume averaged continuum formulation originally proposed by [Bennon and Incropera, 1987a], as shown in below Eqn. 1.

$$\frac{\partial}{\partial t}\left(\sum_k g_k \rho_k h_k\right) + \nabla.\left(\sum_k g_k \rho_k \vec{\mathbf{V}}_k h_k\right) = \nabla.(k\nabla T) \tag{1}$$

Mass averaged enthalpy is defined as $h = f_l h_l + f_s h_s$, where h_s and h_l are the respective phase enthalpies in solid and liquid defined as $h_s = c_{ps}T$ and $h_l = (c_{ps} - c_{pl})T_S + h_{sl} + c_{pl}T$, respectively.

Expanding first term on left hand side of Eqn. 1 we get,

$$\frac{\partial}{\partial t}\left(\sum_k g_k \rho_k h_k\right) = \frac{\partial}{\partial t}(g_l \rho_l h_l + g_s \rho_s h_s) = \frac{\partial}{\partial t}(g_l \rho_l c_{pl} T + g_l \rho_l h_{sl} + g_l \rho_l c_{ps} T_S + g_s \rho_s c_{ps} T) \tag{2}$$

manipulating and arranging the above time derivative terms by adding and subtracting $g_l \rho_l c_{ps} T$ we get,

$$\frac{\partial}{\partial t}\left(\sum_k g_k \rho_k h_k\right) = \frac{\partial}{\partial t}(g_s \rho_s c_{ps} T + g_l \rho_l c_{ps} T + g_l \rho_l h_{sl} + g_l \rho_l c_{pl} T - g_l \rho_l c_{ps} T - g_l \rho_l c_{pl} T_S + g_l \rho_l c_{ps} T_S) \tag{3}$$

$$\frac{\partial}{\partial t}\left(\sum_k g_k \rho_k h_k\right) = \frac{\partial}{\partial t}(\rho c_{ps} T) + \frac{\partial}{\partial t}(g_l \rho_l h_{sl}) + \frac{\partial}{\partial t}\left(g_l \rho_l (c_{pl} - c_{ps})(T - T_s)\right) \tag{4}$$

Expanding second term on left hand side of Eqn. 1 we get,

$$\nabla.\left(\sum_k g_k \rho_k \vec{\mathbf{V}}_k h_k\right) = \nabla.(g_l \rho_l \vec{\mathbf{V}}_l h_l + g_s \rho_s \vec{\mathbf{V}}_s h_s) \tag{5}$$

As velocity in solid domain is assumed to be zero, the term $g_s \rho_s \vec{\mathbf{V}}_s h_s$ is zero and thus $g_l \rho_l \vec{\mathbf{V}}_l = \rho \vec{\mathbf{V}}$. Therefore equation becomes,

$$\nabla.\left(\sum_k g_k \rho_k \vec{\mathbf{V}}_k h_k\right) = \nabla.\left(\rho \vec{\mathbf{V}} c_{pl} T + \rho \vec{\mathbf{V}} h_{sl} + \rho \vec{\mathbf{V}} c_{ps} T_S - \rho \vec{\mathbf{V}} c_{pl} T_S\right) = \nabla.(\rho \vec{\mathbf{V}} c_{pl} T) + (h_{sl} + c_{ps} T_S - c_{pl} T_S)\nabla.(\rho \vec{\mathbf{V}}) \tag{6}$$

$$\nabla.\left(\sum_k g_k \rho_k \vec{\mathbf{V}}_k h_k\right) = \nabla.(\rho \vec{\mathbf{V}} c_{pl} T) - (h_{sl} + c_{ps} T_S - c_{pl} T_S)\frac{\partial \rho}{\partial t} \tag{7}$$

substituting the above expression in Eqn. 1 we get,

$$\frac{\partial}{\partial t}(\rho c_{ps} T) + \nabla.(\rho \vec{\mathbf{V}} c_{pl} T) = \nabla.(k\nabla T) - S \tag{8}$$

where s is the source term and is given as follows

$$S = \frac{\partial}{\partial t}(g_l \rho_l h_{sl}) + \frac{\partial}{\partial t}\left(g_l \rho_l (c_{pl} - c_{ps})(T - T_S)\right) - (h_{sl} + c_{ps} T_S - c_{pl} T_S)\frac{\partial \rho}{\partial t}$$
$$= \frac{\partial}{\partial t}\left(g_l \rho_l h_{sl} + g_l \rho_l (c_{pl} - c_{ps})(T - T_S) - (g_l \rho_l + (1 - g_l)\rho_s)(h_{sl} + c_{ps} T_S - c_{pl} T_S)\right) \quad (9)$$

Simplifying the above expression we get,

$$S = \frac{\partial}{\partial t}((g_l - 1)\rho_s h_{sl}) + \frac{\partial}{\partial t}\left(g_l \rho_l (c_{pl} - c_{ps})T + (1 - g_l)\rho_s (c_{pl} - c_{ps})T_S\right) \quad (10)$$

$$S = \frac{\partial}{\partial t}(g_l \rho_s h_{sl}) + \frac{\partial}{\partial t}\left(g_l (c_{pl} - c_{ps})(\rho_l T - \rho_s T_S)\right) \quad (11)$$

Therefore energy equation is,

$$\frac{\partial}{\partial t}(\rho c_{ps} T) + \nabla.(\rho \vec{\mathbf{V}} c_{pl} T) = \nabla.(k \nabla T) - \frac{\partial}{\partial t}(g_l \rho_s h_{sl}) - \frac{\partial}{\partial t}\left(g_l (c_{pl} - c_{ps})(\rho_l T - \rho_s T_S)\right) \quad (12)$$

Further simplifying the equation in line with requirement we get,

$$\frac{\partial}{\partial t}(\rho T) + \nabla.(\rho \vec{\mathbf{V}} T) = \nabla.\left(\frac{k}{c_{ps}}\nabla T\right) - \nabla.\left[\left(\frac{c_{pl}}{c_{ps}} - 1\right)\rho \vec{\mathbf{V}} T\right] - \frac{\partial}{\partial t}(g_l \rho_s h_{sl})$$
$$- \frac{\partial}{\partial t}\left[g_l \left(\frac{c_{pl}}{c_{ps}} - 1\right)(\rho_l T - \rho_s T_S)\right] \quad (13)$$

2 ENERGY EQUATION FOR PURE AND ALLOY SYSTEM IN PRESENCE OF FREE SURFACE

Rewriting the Eqn. 9 we get,

$$S = \frac{\partial}{\partial t}(g_l \rho_l h_{sl}) + \frac{\partial}{\partial t}\left(g_l \rho_l (c_{pl} - c_{ps})(T - T_S)\right) - (h_{sl} + c_{ps} T_S - c_{pl} T_S)\frac{\partial \rho}{\partial t}$$
$$= \frac{\partial}{\partial t}\left(g_l \rho_l h_{sl} + g_l \rho_l (c_{pl} - c_{ps})(T - T_S) - (g_l \rho_l + g_s \rho_s)(h_{sl} + c_{ps} T_S - c_{pl} T_S)\right)$$
$$= \frac{\partial}{\partial t}\left(g_l \rho_l h_{sl} + g_l \rho_l (c_{pl} - c_{ps})(T - T_S) - (g_l \rho_l + (1 - g_l - g_v)\rho_s)(h_{sl} + c_{ps} T_S - c_{pl} T_S)\right) \quad (14)$$

Simplifying the above expression we get,

$$S = \frac{\partial}{\partial t}((g_l + g_v - 1)\rho_s h_{sl}) + \frac{\partial}{\partial t}\left(g_l \rho_l (c_{pl} - c_{ps})T + (1 - g_l - g_v)\rho_s (c_{pl} - c_{ps})T_S\right) \quad (15)$$

$$S = \frac{\partial}{\partial t}(g_l \rho_s h_{sl}) + \frac{\partial}{\partial t}\left(g_l (c_{pl} - c_{ps})(\rho_l T - \rho_s T_S)\right) + \frac{\partial}{\partial t}(g_v \rho_s h_{sl}) - \frac{\partial}{\partial t}\left(g_v \rho_s (c_{pl} - c_{ps})T_S\right) \quad (16)$$

Further simplifying the equation in line with requirement we get,

$$\frac{\partial}{\partial t}(\rho c_{ps} T) + \nabla.(\rho \vec{\mathbf{V}} c_{pl} T) = \nabla.(k \nabla T) - \frac{\partial}{\partial t}(g_l \rho_s h_{sl}) - \frac{\partial}{\partial t}\left(g_l (c_{pl} - c_{ps})(\rho_l T - \rho_s T_S)\right) - \left(\rho_s h_{sl} - \rho_s (c_{pl} - c_{ps})T_S\right)\frac{\partial g_v}{\partial t} \quad (17)$$

...

Appendix B: SIMPLER algorithm for solution of continuity and momentum equations

The fluid flow calculations performed for all the numerical models presented are obtained by solving continuity and momentum equations using Semi-Implicit Method for Pressure-Linked Equations Revised(SIMPLER) [Patankar, 2018]. A staggered grid arrangement is followed to solve the velocity field as shown in figure B1. The staggered grid arrangement eliminates the difficulties arising by estimating all the variables for the same grid nodes. The velocity flow field is obtained by solving momentum equations whereas the continuity equation is used to define the pressure field. To improve the convergence rate of the iterative method, a revised version has been worked out.

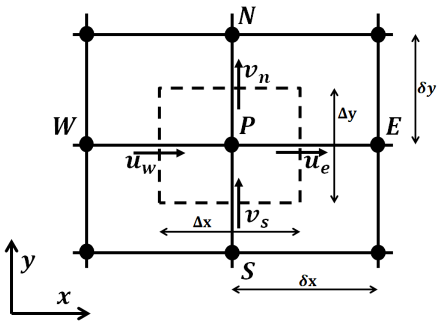

Figure B1 : Control volume for two-dimensional calculations.

A detailed mathematical formulation is given in [Patankar, 2018] and implies following sequence of operations:

1. Initially a flow field is assumed for an entire numerical domain.

2. The momentum equation in its simple form is written as,

$$u_e = \hat{u}_e + d_e(p_P - p_E) \tag{1}$$

where $\hat{u}_e$ and d_e are defined as $\hat{u}_e = (\sum a_{nb}u_{nb} + b)/a_e$ and $d_e = A_e/a_e$ respectively. The term A_e is the area on which pressure difference acts; a_e is the coefficient of the discretised velocity equation; and b is the source term computed at velocity node e.

Calculate coefficients of these momentum equations to obtain $\hat{u}$ and $\hat{v}$ by substituting values of guessed flow field.

3. Once the velocity equation (from step 2) at all the faces are substituted into the discretised continuity equation, a pressure equation is obtained.

$$a_P p_P = \sum a_{nb} p_{nb} + b \tag{2}$$

where b in Eqn. 2 is given as

$$b = \frac{(\rho_P^0 - \rho_P)\Delta x \Delta y}{\Delta t} + [(\rho\hat{u})_w - (\rho\hat{u})_e]\Delta y + [(\rho\hat{v})_s - (\rho\hat{v})_n]\Delta x \tag{3}$$

Evaluate the values of the coefficients of the pressure equation Eqn. 1; $a_E = \rho_e d_e \Delta y$, $a_W = \rho_w d_w \Delta y$, $a_N = \rho_n d_n \Delta x$, and $a_S = \rho_s d_s \Delta x$. Eqn. 2 is then solved to obtain the pressure field.

4. The obtained pressure field is then treated as guess pressure field p^* to solve the discretised momentum equations,

$$a_e u_e^* = \sum a_{nb} u_{nb}^* + b + (p_P^* - p_E^*) A_e \tag{4}$$

$$a_n v_n^* = \sum a_{nb} v_{nb}^* + b + (p_P^* - p_N^*) A_n \tag{5}$$

   Solving the equations we get u^* and v^*

5. Using u^* and v^*, the pressure correction equation is solved to obtain the values for p'.

$$a_P p_P' = \sum a_{nb} p_{nb}' + b \tag{6}$$

   where coefficients a_P and a_{nb} are the same evaluated for pressure equation; and b is defined as

$$b = \frac{(\rho_P^0 - \rho_P)\Delta x \Delta y}{\Delta t} + [(\rho u^*)_w - (\rho u^*)_e]\Delta y + [(\rho v^*)_s - (\rho v^*)_n]\Delta x \tag{7}$$

6. Using velocity correction formula as given

$$u_e = u_e^* + d_e(p_P' - p_E') \tag{8}$$

$$v_n = v_n^* + d_n(p_P' - p_N') \tag{9}$$

   correct the flow field, but pressure correction is unnecessary.

7. Once flow field is obtained, solve dicreatised equations for other scalar quantities viz., temperature T and concentration C, respectively.

8. Repeat the procedure from step 2 until desired convergence is obtained.

...

Appendix C: Volume of Fluid Method

For the present investigation a volume of fluid (VOF) method is implemented to track the interface motion between solidifying melt and void section. The method is implemented to obtain the void fraction g_v, by solving the advection equation (Eqn. 1). Since the flow field conserves the shape and void fraction volume, g_v satisfies the advection equation,

$$\frac{\partial}{\partial t}(g_v) + \nabla.(g_v \mathbf{V}) = g_v (\nabla.\mathbf{V}) \tag{1}$$

Further to solve the eqn. 1, the operator splitting method is employed that results into two different equations varying in x and y direction independently [Gerlach et al., 2006; Puckett et al., 1997].

$$\frac{\partial}{\partial t}(g_v) + \frac{\partial}{\partial x}(g_v u) = g_v \frac{\partial u}{\partial x} \tag{2}$$

$$\frac{\partial}{\partial t}(g_v) + \frac{\partial}{\partial y}(g_v v) = g_v \frac{\partial v}{\partial y} \tag{3}$$

In order to sustain the conservation of void fraction g_v it is required to discretise implicitly on right hand side of eqn. 2 and explicitly on right hand side of eqn. 3. Use of implicit-explicit scheme in alternate sweep directions assists in obtaining the second order accuracy. The final discretised equations are given below with reference to figure C1(a),

$$(g_v')_{i,j} = \left[(g_v^n)_{i,j} + \frac{1}{\Delta x}\left(\delta F_{i-1/2,j} - \delta F_{i+1/2,j}\right)\right] / \left[1 - \frac{\Delta t}{\Delta x}\left(u_{i-1/2,j} - u_{i+1/2,j}\right)\right] \tag{4}$$

$$(g_v^{n+1})_{i,j} = (g_v')_{i,j}\left[1 + \frac{\Delta t}{\Delta y}\left(v_{i,j+1/2} - v_{i,j-1/2}\right)\right] + \frac{1}{\Delta y}\left(\delta F'_{i,j-1/2} - \delta F'_{i,j+1/2}\right) \tag{5}$$

where δF is the amount of liquid void fraction that is fluxed through the cell face. The superscript ($'$) used in eqn. 5 simply denotes the void flux value at intermediate stage after the first sweep in x-direction.

The important operation is now to calculate the δF for the above discretised eqns. 4 and 5 in such a manner that the conservation of void fraction is followed and no numerical augmentation is instigated. This is performed by following the donor-acceptor scheme proposed by Hirt and Nichols [1981]. Figure C1(b) considers the fluid flow configuration with a positive fluid flow in x-direction at face $i + \frac{1}{2}$. The donor-acceptor method estimates the volume flux across node $(i + \frac{1}{2}, j)$ as,

$$\delta F_{i+1/2,j} = \Delta y \Big\{ \text{MIN}\Big[(g_v)_{i,j}\delta x, u_{i+1/2,j}(g_v)_{i+1,j}\delta t + \text{MAX}\Big(0.0, u_{i+1/2,j}(1-(g_v)_{i+1,j})\delta t - (1-(g_v)_{i,j})\delta x\Big)\Big]\Big\} \tag{6}$$

The MIN feature in eqn. 6 prevents the additional fluxing of fluid from cell (i, j) through face $(i + \frac{1}{2}, j)$ whereas the max feature ensures that no more void volume is fluxed out of cell (i, j).

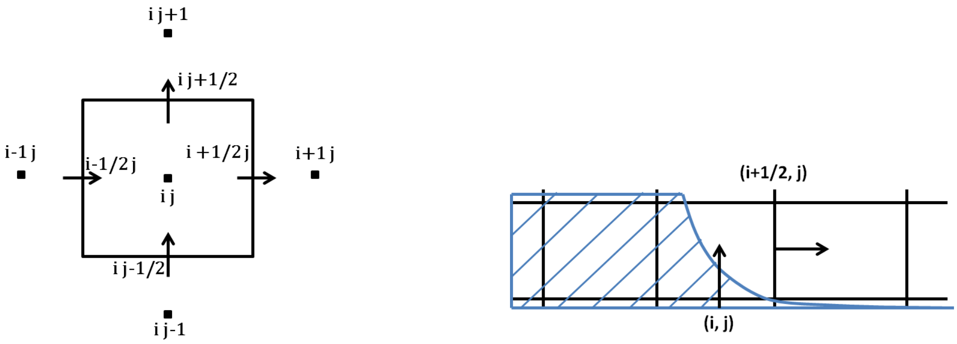

(a) (b)

Figure C1 : (a) Discretised representation of control volume and (b) Interface configuration for Hirt-Nichols VOF model.

…

Appendix D: List of publications from the present investigation

D1 JOURNAL ARTICLES

1. Monde AD, Shrivastava A, Jakhar A, Chakraborty PR. "Binary alloy solidification and freckle formation: Effect of shrinkage induced flow on solutal instability and macro-segregation" *Physics of Fluids. 2021 Mar 1;33(3):037108*.

2. Monde AD, Chawla O, Kumar V, Karagadde S, Chakraborty PR. "Shrinkage induced flow during directional solidification of pure substance in a bottom cooled cavity: A study on flow reversal phenomena" *Physics of Fluids 2020 Apr 1;32(4):047104*.

3. Monde AD, Chakraborty PR. "Prediction of cooling curves for controlled unidirectional solidification under the influence of shrinkage: a semi-analytical approach" *Metallurgical and Materials Transactions B. 2018 Dec 1;49(6):3306-16*.

4. Monde AD, Chakraborty PR. "1-D diffusion based solidification model with volumetric expansion and shrinkage effect: A semi-analytical approach" *Physics Letters A. 2017 Oct 17;381(39):3349-54*.

D2 CONFERENCES

1. Monde AD, Jakhar A, Chakraborty PR."Effect of shrinkage during thermo-solutal convection for a unidirectional solidification of binary alloys" *8th International and 47th National Conference on Fluid Mechanics and Fluid Power (FMFP-2020) 2020*

2. Monde AD, Chawla O, Chakraborty PR. "Numerical Analysis of Shrinkage Induced Convection during Bottom up Solidification of Pure Material" *25th National and 3rd International ISHMT-ASTFE Heat and Mass Transfer Conference (IHMTC-2019) 2019*

3. Monde AD, Bhattacharya A, Chakraborty PR. "Shrinkage induced flow and Free surface evolution during solidification of pure metal" *In E3S Web of Conferences 2019 (Vol. 128, p. 06011). EDP Sciences*.

4. Kumar C, Monde AD, Bhattacharya A, Chakraborty PR. "Modeling of dendrite growth in undercooled solution sodium acetate trihydrate" *In E3S Web of Conferences 2019 (Vol. 128, p. 01023). EDP Sciences*.

5. Monde AD, Chawla O, Bhuyar V, Vijay M, Chakraborty PR. "Performance evaluation of latent heat based cool pack configuration for thermal comfort: A numerical approach" *International Conference on Computational Methods for Thermal Problems 2018*